Monthly Notices
of the
ROYAL ASTRONOMICAL SOCIETY

MNRAS **492,** 2683–2697 (2020)
Advance Access publication 2020 January 3

doi:10.1093/mnras/stz3603

Are exoplanetesimals differentiated?

Amy Bonsor,[1]★ Philip J. Carter,[2] Mark Hollands,[3] Boris T. Gänsicke,[3] Zoë Leinhardt[4] and John H. D. Harrison[1]

[1]*Institute of Astronomy, University of Cambridge, Madingley Road, Cambridge CB3 0HA, UK*
[2]*Department of Earth and Planetary Sciences, University of California Davis, One Shields Avenue, Davis, CA 95616, USA*
[3]*Department of Physics, University of Warwick, Coventry CV4 7AL, UK*
[4]*School of Physics, HH Wills Physics Laboratory, University of Bristol, Tyndall Avenue, Bristol BS8 1TL, UK*

Accepted 2019 December 18. Received 2019 December 13; in original form 2019 November 1

ABSTRACT

Metals observed in the atmospheres of white dwarfs suggest that many have recently accreted planetary bodies. In some cases, the compositions observed suggest the accretion of material dominantly from the core (or the mantle) of a differentiated planetary body. Collisions between differentiated exoplanetesimalrrs produce such fragments. In this work, we take advantage of the large numbers of white dwarfs where at least one siderophile (core-loving) and one lithophile (rock-loving) species have been detected to assess how commonly exoplanetesimals differentiate. We utilize *N*-body simulations that track the fate of core and mantle material during the collisional evolution of planetary systems to show that most remnants of differentiated planetesimals retain core fractions similar to their parents, while some are extremely core rich or mantle rich. Comparison with the white dwarf data for calcium and iron indicates that the data are consistent with a model in which 66^{+4}_{-6} per cent have accreted the remnants of differentiated planetesimals, while 31^{+5}_{-5} per cent have Ca/Fe abundances altered by the effects of heating (although the former can be as high as 100 per cent, if heating is ignored). These conclusions assume pollution by a single body and that collisional evolution retains similar features across diverse planetary systems. These results imply that both collisions and differentiation are key processes in exoplanetary systems. We highlight the need for a larger sample of polluted white dwarfs with precisely determined metal abundances to better understand the process of differentiation in exoplanetary systems.

Key words: planets and satellites: general – circumstellar matter – planetary systems – white dwarfs.

1 INTRODUCTION

Elements heavier than helium sink below the observable atmospheres of white dwarfs on time-scales of days (young, hydrogen-rich, or DA white dwarfs) to millions of years (old, helium-rich, or DB white dwarfs) (Koester 2009). The presence of heavy elements in the atmospheres of >30 per cent of white dwarfs (Zuckerman et al. 2003, 2010; Koester, Gänsicke & Farihi 2014) can only be explained by their recent or ongoing accretion. The consensus in the literature is that we are observing the accretion of planetary bodies that have survived the star's evolution in an outer planetary system orbiting the white dwarf (e.g. Jura 2003; Farihi 2016; Veras 2016). Dynamical instabilities following stellar mass-loss can scatter planetary bodies on to star-grazing orbits (Debes & Sigurdsson 2002; Bonsor, Mustill & Wyatt 2011; Debes, Walsh & Stark 2012; Veras et al. 2013) where they are disrupted by strong tidal forces (Veras et al. 2014). Fragments of disrupted bodies are accreted on to the star, with observations of gas and dust tracing this accretion in action (see Farihi 2016 for a recent review).

The abundances observed in the atmospheres of white dwarfs provide unique insights regarding the composition of exoplanetary building blocks – the planetesimals accreted by the white dwarfs. While most white dwarf pollutants exhibit abundances that are broadly similar to rocky planets (Jura & Young 2014), a handful show the presence of volatiles, including oxygen and nitrogen (e.g. Farihi et al. 2011; Raddi et al. 2015; Xu et al. 2017). High abundances of refractory species, such as calcium and titanium, have led to the suggestion that some white dwarf pollutants experienced high-temperature processing, similar to meteorites from the inner Solar system, for example, G29−38 (Xu et al. 2014). Extreme abundances of either siderophile (core-loving) species, i.e. iron, or lithophile (rock-loving) species, such as calcium, magnesium,

★ E-mail: amy.bonsor@gmail.com

or silicon, have led to the suggestion that these polluted white dwarfs have accreted a fragment of a larger body that differentiated into a core and a mantle. For example, for SDSS J0845+2257 (Wilson et al. 2015), the high iron abundance could be explained by the accretion of a planetesimal stripped of its mantle. In order to explain the observed abundances, not only must the planetary bodies differentiate but also collisions must be sufficiently catastrophic that at least some fragments have extreme compositions, e.g. core rich.

Both collisions and differentiation are common features of our asteroid belt. Samples of differentiated bodies arrive to Earth as meteorites, most famously the iron meteorites. The range of different spectral classifications for asteroids could be explained in part by their differentiation and collisional evolution (Burbine et al. 2002). The budget of short-lived radioactive nuclides in the Solar system, including ^{26}Al, is sufficient to differentiate bodies larger than >10 km (Urey 1955; Ghosh & McSween 1998), and there is a growing suite of evidence that differentiation occurred early (Kleine et al. 2005; Scherstén et al. 2006; Kruijer et al. 2014). We note here that there is sufficient potential energy imparted during formation alone to differentiate bodies larger than around 1000 km, without the need for short-lived radioactive nuclides (e.g. Davison, Collins & Ciesla 2010; Elkins-Tanton, Weiss & Zuber 2011). In fact, the differentiation of planetary building blocks influences not only the composition of the terrestrial planets, most notably the budgets of highly siderophile elements (Rubie et al. 2011, 2015; Fischer, Campbell & Ciesla 2017), but also potentially the bulk composition (Bonsor et al. 2015; Carter et al. 2015). However, the budget of short-lived radioactive nuclides in exoplanetary systems is greatly debated (e.g. Boss & Keiser 2010; Gritschneder et al. 2012; Young 2014; Gounelle 2015; Lichtenberg, Parker & Meyer 2016) and it is not clear how widespread the differentiation of small exoplanetary bodies is. In fact, Jura, Xu & Young (2013) previously used the white dwarf observations to suggest that the Solar system's abundance of ^{26}Al was not so unusual.

Collisions between differentiated bodies can lead to fragments with a diverse range of compositions. Simulations of disruptive collisions produce fragments with a range of compositions, including those dominated by core material or mantle material (Marcus et al. 2010; Bonsor et al. 2015; Carter et al. 2015). Mercury could be a collision fragment dominated by core material, stripped of its mantle in a high-velocity collision (Benz, Slattery & Cameron 1988). The merging of planetary cores and the stripping of mantles are common features of high-velocity collisions (Benz et al. 1988; Marcus et al. 2009; Landeau et al. 2016). Similar processes have been hypothesized to occur in exoplanetary systems (Marcus et al. 2009). In this work, we consider how the differentiation and collisional evolution of planetesimal belts may influence the compositions of planetary bodies accreted by white dwarfs.

With the growing number of *polluted* white dwarfs where both lithophile (e.g. calcium) and siderophile (e.g. iron) elements have been detected, it is now possible to assess the population of exoplanetary systems as a whole. We hypothesize that all polluted white dwarfs have accreted planetesimals from outer planetesimal belts that have survived the star's evolution. These outer planetesimal belts are commonly observed around main-sequence stars and known to be collisionally active due to the large quantities of small dust continuously replenished in collisions between larger bodies (Wyatt 2008; Hughes, Duchene & Matthews 2018). Collisions between planetesimals that have differentiated to form a core and a mantle should lead to a spread in total abundances of siderophile (e.g. iron) and lithophile (e.g. calcium) species. If polluted white dwarfs sample this distribution, it will be reflected by the spread in their observed calcium and iron abundances.

The aim of this work is to collate as large a sample as possible of polluted white dwarfs where both calcium and iron are detected and use these, compared to models for the collisional evolution of differentiated planetesimals, to infer the prevalence of differentiation in exoplanetesimals. Do most planetary systems have planetesimals that differentiate, or is the differentiation of planetesimals a unique feature of the Solar system?

We start by summarizing the aims and approach of this paper in Section 2, followed by the observational data sample in Section 3. In Section 4, we first consider the possibility that the distribution of abundances could be explained by a range of initial abundances for the planet-forming material. In Section 5, we compare the white dwarf observations to the results of the simulations and investigate the frequency of differentiation in the observed white dwarf planetary systems. In Section 6, we discuss the overabundance of polluted white dwarfs with above average Ca/Fe ratios and suggest that this trend may be related to the temperatures experienced by the planetesimals. In Section 7, we discuss what can be concluded by the currently available data and models, before summarizing our conclusions in Section 8.

2 AIMS AND APPROACH

In this work, we aim to investigate what the observed population of polluted white dwarfs can tell us about how frequently exoplanetesimals are differentiated. We do this by comparing the observed population to a model population, developed from the results of simulations. The *N*-body simulations follow the collisional evolution of planetary systems, tracing the fate of core-like and mantle-like material. We use collision simulations to predict the population of fragments that accrete on to white dwarfs and compare to the observed population of white dwarf pollutants.

Calcium and iron are both commonly observed in polluted white dwarfs, while being a pair of lithophile and siderophile elements that behave differently during differentiation. In addition to that, both elements sink at relatively similar time-scales through the white dwarf atmosphere (Koester 2009), which means that the observed abundances should match those of the material accreted on to the star and do not need to be adjusted to take into account differential sinking. The ratio of Ca to Fe should remain unchanged even if the sinking time-scales change, for example in hot DA white dwarfs due to the onset of thermohaline (fingering) convection sinking time-scale may be significantly longer (Deal et al. 2013; Zemskova et al. 2014; Wachlin et al. 2017; Bauer & Bildsten 2018, 2019) or accreted material is mixed much deeper into the white dwarf (Cunningham et al. 2019).

Ca and Fe are, therefore, a very useful pair of species for diagnosing the levels of differentiation in exoplanetesimals. We collate as large an observational sample as possible of white dwarfs where both calcium and iron have been detected and compare these to the model predictions. We utilize the cumulative distribution of Ca/Fe ratios, **k**, to compare the model to the observations. For the observations, this essentially equates to a list of observed Ca/Fe values in ascending order, each with an associated error, $\sigma_{\mathrm{Ca/Fe}}$. We, therefore, define $X^{\mathrm{obs}}_{\mathrm{Ca/Fe}}(\mathbf{k})$ as the value of Ca/Fe for which a fraction **k** of the observed sample have a lower Ca/Fe measurement, or in other words a fraction **k** of the sample have an observed Ca/Fe ratio lower than $X^{\mathrm{obs}}_{\mathrm{Ca/Fe}}(\mathbf{k})$. In a similar manner, a fraction **k** of the model population are predicted to have a lower Ca/Fe value than

$X^{\rm model}_{\rm Ca/Fe}(\mathbf{k})$. We can, thus, assess the quality of the model fit using a reduced chi-squared of

$$\chi^2_{\rm model} = \frac{1}{N_{\rm WD}} \sum_{k=0}^{1} \left(\frac{X^{\rm model}_{\rm Ca/Fe}(\mathbf{k}) - X^{\rm obs}_{\rm Ca/Fe}(\mathbf{k})}{2\sigma_{\rm Ca/Fe}(\mathbf{k})} \right)^2, \quad (1)$$

where $N_{\rm WD}$ is the number of white dwarfs in the sample.

In order to determine the most likely values of the model parameters, we use a Bayesian framework. The posterior probability distribution $[p(\theta|M_i,\ D)]$ of the model parameters θ, given the model M_i and the data D, is proportional to the likelihood of the data, given the model and parameters $L(D|\theta,\ M_i)$ and the prior on the model parameters $p(\theta|M_i)$ (see Section 5.2 and Section 6.1). In order to answer the question whether exoplanetesimals are differentiated, the key model parameter (θ) is the fraction of exoplanetesimals that are differentiated, $f_{\rm diff}$. The Markov Chain Monte Carlo (MCMC) fitting routine (Foreman-Mackey et al. 2013) is used to maximize this likelihood function in order to find posterior distribution for each model parameter, assuming a likelihood of the form

$$\begin{aligned} &L(X^{\rm obs}_{\rm Ca/Fe}|\theta,\ M_i) \\ &= \prod_{k=0}^{1} \frac{1}{\sqrt{2\pi}\sigma_{\rm Ca/Fe}(\mathbf{k})} \exp\left(-\left(\frac{X^{\rm model}_{\rm Ca/Fe}(\mathbf{k}) - X^{\rm obs}_{\rm Ca/Fe}(\mathbf{k})}{2\sigma_{\rm Ca/Fe}(\mathbf{k})} \right)^2 \right) \\ &\times ln\ L(X^{\rm obs}_{\rm Ca/Fe}|\theta,\ M_i) \\ &-\sum_{k=0}^{1} \left(\ln(\sqrt{2\pi}\ \sigma_{\rm Ca/Fe}(\mathbf{k})) + \left(\frac{X^{\rm obs}_{\rm Ca/Fe}(\mathbf{k}) - X^{\rm model}_{\rm Ca/Fe}(\mathbf{k})}{2\sigma_{\rm Ca/Fe}(\mathbf{k})} \right)^2 \right). \end{aligned} \quad (2)$$

3 OBSERVATIONAL DATA

The observational samples are collated from the literature; some are the most highly polluted white dwarfs where multiple species have been detected (Klein et al. 2011; Zuckerman et al. 2011; Dufour et al. 2012; Gänsicke et al. 2012; Jura et al. 2012; Kawka & Vennes 2012, 2016; Farihi, Gänsicke & Koester 2013; Xu et al. 2013; Raddi et al. 2015; Wilson et al. 2015; Farihi et al. 2016; Hollands et al. 2017; Swan et al. 2019), while most are cool ($T_* < 9000$ K) DZs from Hollands et al. (2017) and Hollands, Gänsicke & Koester (2018). Errors on the measured abundances are taken from the literature, where available [$\sigma_{\rm Ca}$ is the error on $10^{\rm Ca/H(e)}$ and $\sigma_{\rm Fe}$ on $10^{\rm Fe/H(e)}$]. We note that quoted errors are often conservative, with an attempt to fold in uncertainties on the atomic data, as well as uncertainties derived from models of the white dwarf atmospheres. Standard error propagation is used to find the error on the Ca/Fe ratio, assuming that the errors on the Ca and Fe abundances are independent: $\sigma_{\rm Ca/Fe} = \frac{10^{\rm Ca/H(e)}}{10^{\rm Fe/H(e)}} \ln(10)(\sigma^2_{\rm Ca} + \sigma^2_{\rm Fe})^{1/2}$. This may not be valid as abundances in Ca and Fe may be correlated. For the Hollands et al. (2017) sample, errors are estimated assuming that they are a sum of systematic errors plus the statistical uncertainty on the abundances, where the systematic errors for Ca and Fe are taken to be $\sigma_{\rm Ca,\ sys} = \sigma_{\rm Fe,\ sys} = 0.05$ dex and $\sigma^2_{\rm Ca} = \sigma^2_{\rm Ca,sys} + \left(\frac{1.27}{\rm (S/N)}\right)^2$, and an equivalent equation for $\sigma^2_{\rm Fe}$, where S/N is the mean spectral signal-to-noise ratio between 4500 and 5500 Å, taken from Hollands (private communication) and the scaling factor 1.27 is a conservative estimate, based on the weakest lines in the noisiest spectra matching the maximum error on an individual element detection (Hollands et al. 2017). For those white dwarfs with low signal-to-noise observations, particularly from Hollands et al. (2017), the Ca and Fe abundances are poorly known and do not provide information regarding differentiation. We, therefore, focus on a sample of white dwarfs where S/N > 5 in this work (as suggested by Hollands et al. 2018), which includes 179 white dwarfs. Fig. 1 plots the observed Ca and Fe abundances, alongside associated errors. Table A1 lists the Ca and Fe abundances of the sample with associated errors, stellar temperatures, and references for all measurements.

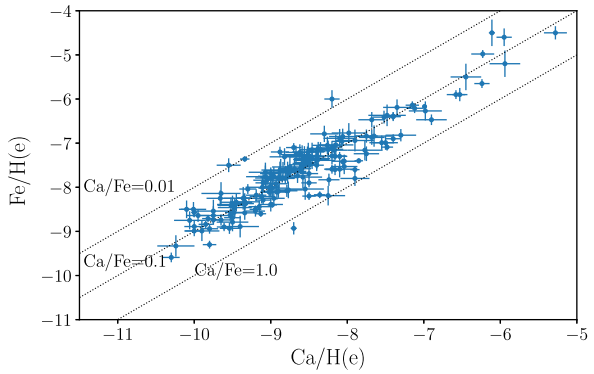

Figure 1. The calcium and iron abundances measured in the 179 white dwarfs plotted in the sample. Lines of constant Ca/Fe ratio are overplotted as dotted lines.

4 A RANGE OF INITIAL ABUNDANCES IN THE PLANET-FORMING MATERIAL

In the scenario that no exoplanetesimals differentiate, a narrow range in the Ca/Fe ratios of exoplanetesimals is expected resulting from the narrow range of Ca/Fe ratios found in the initial conditions of the material from which these planetesimals formed. If we consider that stars and planetary systems form out of the same material, then we can assume that the range of compositions of nearby stars will be fairly similar to the range of initial compositions present in their planetary systems. We can easily determine the compositions of nearby stars, whereas determining the initial compositions of their planetary systems is challenging. We, therefore, consider the range of Ca/Fe ratios found in a sample of nearby stars to be a good proxy for the potential spread expected for undifferentiated, pristine exoplanetesimals. We compare the cumulative distribution of Ca/Fe ratios found in a sample of nearby FGK stars taken from Brewer et al. (2016) to the population of polluted white dwarfs. FGK stars are used as they are more likely to have formed at similar times, thus, with potentially similar compositions, to the progenitors of the white dwarfs considered. Fig. 2 shows the cumulative distribution of Ca/Fe ratios observed in polluted white dwarfs (magenta line), along with a corresponding error range shown in grey. This is calculated by considering the cumulative distribution that would occur if all white dwarfs in the sample were measured to have their measured Ca/Fe (de)increased by one sigma. This is compared to the distribution of Ca/Fe ratios seen in nearby stars (black line). The polluted white dwarfs show a much broader range of Ca/Fe ratios. We find a reduced $\chi^2_{\rm stellar} = 3.5$, indicating a relatively poor fit. If we consider those 35 white dwarfs with S/N > 20, $\chi^2_{\rm stellar} = 12.5$ and this is clearly a bad model for the observational data.

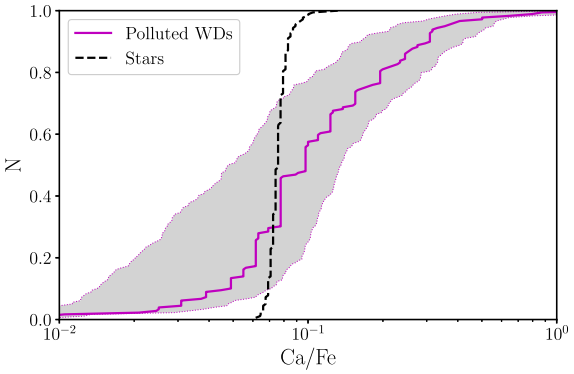

Figure 2. The cumulative distribution of Ca/Fe ratios observed in the white dwarf pollutants (magenta solid line, plus grey shaded region indicating 1 − σ errors), compared to the cumulative distribution of Ca/Fe abundances predicted for the scenario in which no exoplanetesimals differentiate (stars: black dashed line).

5 COLLISIONS BETWEEN DIFFERENTIATED PLANETESIMALS

Planetesimal belts evolve over many billions of years to the white dwarf phase. Debris discs around main-sequence stars provide evidence that planetesimal belts are collisionally active (Wyatt 2008). If the planetesimals have differentiated to form a core and a mantle, collisions between these differentiated planetesimals lead to fragments with a range of compositions and, of particular relevance here, a range of Ca/Fe ratios (Marcus et al. 2009, 2010; Bonsor et al. 2015; Carter et al. 2015). The scattering and accretion of planetesimals from planetary systems that have survived the star's main-sequence evolution to the white dwarf phase is thought to be a dynamical process (Veras 2016) and thus broadly independent of a body's collisional or geological history. Thus, we anticipate that if the exoplanetesimals accreted by white dwarfs originate from a system where both collisions and differentiation have occurred, they should randomly sample this distribution of Ca/Fe ratios.

The aim here is to produce a model population that predicts the distribution of Ca/Fe ratios following collisional evolution and random sampling of the collision fragments by the white dwarfs. The exact distribution of Ca/Fe ratios will depend upon the precise architecture, in particular orbital location of material and evolution time-scales, of individual systems. Given that it is not computationally feasible to consider the full range of system architectures, we use a single system as a proxy for all systems. We base our results on the simulations of our own Solar system, early in its evolution, namely considering a planetesimal belt in the region around Earth's orbit. While this system goes on to form some protoplanets, it leaves behind a population of collision remnants, produced from a range of destructive and constructive collisions. We use these remnants as a proxy for the bodies accreting on to the white dwarfs.

We hypothesize that if the distribution of Ca/Fe ratios in collision fragments is broadly similar across all planetary systems, the result of the polluted white dwarfs sampling a range of systems will be similar to our model in which a single system is sampled. Crucially, we note that even if the distribution of Ca/Fe ratios exhibits stark differences between individual systems, these will be very difficult to disentangle from the general population and therefore, as a first approach, we can derive significant insights from our model.

In particular, we anticipate that similar evolution will occur on longer time-scales further from the star. We simulate a massive belt (see below), close to the star (∼1 au) such that the collisional evolution occurs rapidly. However, if we consider that collisions are dominated by catastrophic collisions, Wyatt et al. (2007) and Wyatt (2008) estimate that the collisional time-scale is proportional to the belt orbital radius, r as $r^{13/3}$, such that the evolution occurring in a belt at 1 au in 10 Myr occurs at 5 au in approximately 10 Gyr. Thus, we anticipate that the distribution from a close-in system on short time-scales can be used as a proxy for the distribution from a system further out on longer time-scales, potentially more relevant to planetary systems around white dwarfs. We note here that most collisional evolution will occur while the planetary systems are on the main sequence, while some evolution may continue during the white dwarf phase, at which point the system will have expanded in orbital radii, potentially by a factor of ∼3 due to the reduced stellar mass. The use of a single system at a single epoch to represent the sampling of a range of systems on a range of time-scales by the white dwarfs can be justified if the initial evolution of the Ca/Fe distribution is more dramatic than the evolution on longer collision time-scales. We will discuss the time dependence of the distribution of Ca/Fe ratios in remnant planetesimals in further detail in Section 7.1.

To summarize, while we hypothesize that the white dwarfs are polluted by planetesimals resulting from a wide range of different planetary systems with different architectures and collision histories, we use a single system as a proxy to predict the distribution of Ca/Fe ratios in the population of planetesimals polluting white dwarfs. This assumes that the generic form of the predicted distribution of Ca/Fe ratios can be applied across a wide range of systems and we, therefore, try not to pin our conclusions down to the specific details of the distribution predicted here.

5.1 Simulations

The *N*-body simulations were performed using a state-of-the-art *N*-body code, PKDGRAV. The collisional evolution of a planetesimal belt is followed, taking into account both destructive and accretional collisions. The fate of collision fragments is tracked using the EDACM collision model (Leinhardt et al. 2015). Every planetesimal is assumed to start with a given size and initial core mass fraction. The fate of core and mantle material during collisions is tracked separately using prescriptions based on simulations of Marcus et al. (2009, 2010). Full details of the code and simulations can be found in Leinhardt et al. (2015), Bonsor et al. (2015), and Carter et al. (2015). The simulations were originally designed to focus on terrestrial planet formation in the inner regions of planetary systems and, therefore, lead to the formation of several protoplanets. For the purposes of this work, we focus on the collisionally evolved population of fragments that remain at the end of the simulations, only considering bodies with a mass less than 0.1 $M_{\oplus}$. This population will have undergone similar collisional evolution to that which might occur in a planetesimal belt. The formation of protoplanets can *stir* the smaller fragments, inciting further collisional evolution, in a similar manner as is thought to occur in outer debris discs either due to self-stirring or planet stirring (Wyatt 2008; Mustill & Wyatt 2009; Kennedy & Wyatt 2010). For a planetesimal belt significantly further from the star, or significantly less dense, the evolution seen in these simulations is representative of the evolution that would occur on significantly longer time-scales, time-scales that would be computationally infeasible to simulate. Each simulation takes about 1 month to run. Two types of collision

simulations are considered; the first considers Earth formation in a *Calm* scenario and was repeated five times, while the second considers a more specialized scenario involving Earth's formation, but this time including Jupiter's Grand Tack (GT). Full details of both scenarios can be found in Carter et al. (2015):

(i) **Calm:** The evolution of 100 000 planetesimals with an initial radius of between 196 and 1530 km in a belt of 2.5 $M_\oplus$ between 0.5 and 1.5 au is followed for 20 Myr.[1] All planetesimals start with an initial core mass fraction of $C_f(0) = 0.35$. These are equivalent to Simulations 8–11 (*Calm* 1–4), as labelled in Carter et al. (2015). The remaining difference between the simulations depends on the exact laws used to determine the fate of core and mantle material following collisions.

(ii) **Grand Tack:** The evolution of 10 000 planetesimals with an initial radius of between 528 and 2250 km in a belt of 4.85 $M_\oplus$ between 0.5 and 3.0 au is followed for 20 Myr.[1] The migration of a Jupiter mass planet in a so-called GT is included, where Jupiter starts at 3.5 au, migrates inwards to 1.5 au, and then back outwards to finish at 5.2 au. Gas drag is included with a surface density profile based on hydrodynamical simulations of giant planets embedded in a disc (Morbidelli & Crida 2007). The effect of Jupiter's GT is essentially to increase collision velocities, in a similar manner as might occur later in the evolution of a planetary system due to other effects, including stirring by a giant planet (Simulation 28 in Carter et al. 2015).

In both simulations, a range of collision fragments are created following each (partially) destructive collision. Fragments that fall below the minimum resolution limit (196 km for the *Calm* simulations) are added to the mass in unresolved dust. This debris is distributed in a series of circular annuli each 0.1 au wide, with the debris placed in the annulus corresponding to the location of the collision that produced it. This material is assumed to have circular Keplerian orbits. The unresolved debris is accreted on to all planetesimals at each time-step, and the fraction of core and mantle material in the unresolved debris is tracked. Given that mantle stripping is common for small fragments, this unresolved debris tends to be dominated by mantle material and leads to all fragments accreting extra mantle-like material.

5.1.1 *Distribution of core mass fractions*

In this work, we are interested in the collisionally evolved fragments and their range of potential abundances. We, therefore, focus on the distribution of core mass fractions of planetesimals, with masses less than 0.1 $M_\oplus$, that survive to the end of the simulations. Fig. 3 shows these distributions. All the simulations display two key features that were also seen in other similar simulations with different initial parameters. First, the distribution of core mass fractions is peaked close to the initial core mass fraction of the planetesimals. Secondly, the simulations produce a wide range of fragments, spread between core-rich and mantle-rich fragments, with the potential for some fragments that are extremely core rich or mantle rich.

In these simulations, the peak in the distribution is always shifted slightly towards mantle-rich fragments. This can be attributed to two effects. First, the prescription used in Carter et al. (2015)

[1]This is the effective time elapsed, which differs from the time for which the simulation was run by a correction to take into account the expanded radii particles used in order to speed the computation by a factor of 6. See Carter et al. (2015) for more details.

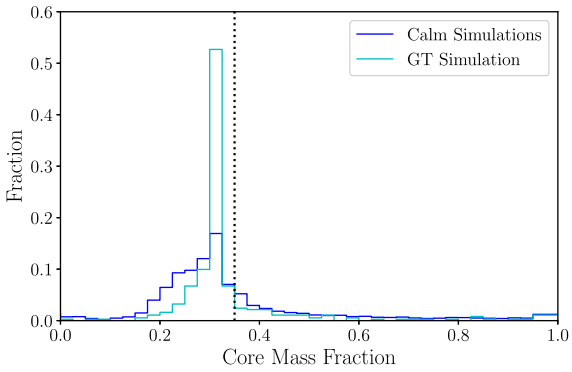

Figure 3. The distribution of core mass fractions for fragments with masses less than 0.1 $M_\oplus$ left at the end of the *N*-body simulations (see Section 5.1). The four *Calm* simulations are averaged for clarity. The dotted line indicates the initial core mass fraction of $C_f(0) = 0.35$ given to planetesimals.

favours the accretion of cores by the largest remnants following a collision. This leads to the core material being predominantly found in the larger, less numerous remnants, such that most remnants tend towards being more mantle rich. Secondly, most bodies have grown by accreting the predominantly mantle rich, unresolved fragments, which fill the orbital parameter space around the original bodies. Whether this is a realistic effect or a result of the limited resolving power of the simulations that can only track planetesimals down to around 200 km in size (see Section 5.1 for details) remains unclear. The main difference between the Calm simulations and the GT simulations is that in the GT simulations the core mass distribution is more highly peaked. Jupiter excites the planetesimals such that there are more disruptive collisions, which produce more debris. As collisions are more disruptive, this debris contains more core material and thus the accretion of this debris leads to a population of fragments with core mass fractions very close to the average values.

In order to compare the simulation results to the white dwarf observations, we convert the distribution of core mass fractions to a distribution of Ca/Fe ratios in the simplest manner possible, by assuming that the mass fractions of Ca and Fe in the planetesimal's core and mantle are the same as in bulk Earth, respectively. This means that

$$\left(\frac{\mathrm{Ca}}{\mathrm{Fe}}\right)_{\mathrm{sims}} = \left(\frac{A_{\mathrm{Fe}}}{A_{\mathrm{Ca}}}\right)\left(\frac{(1-C_{\mathrm{f}})\mathrm{Ca}^{\oplus}_{\mathrm{mantle}}}{C_{\mathrm{f}}\mathrm{Fe}^{\oplus}_{\mathrm{core}} + (1-C_{\mathrm{f}})\mathrm{Fe}^{\oplus}_{\mathrm{mantle}}}\right), \quad (3)$$

where C_f is the core mass fraction of the planetesimal, A_{Fe} and A_{Ca} are the atomic weights for iron and calcium, $\mathrm{Ca}^{\oplus}_{\mathrm{mantle}} = 26.1 \times 10^{-3}$ the mass fraction of Ca in Earth's mantle, $\mathrm{Fe}^{\oplus}_{\mathrm{core}} = 0.85$ the mass fraction of iron in the core, and $\mathrm{Fe}^{\oplus}_{\mathrm{mantle}} = 0.063$ (all values from Palme & O'Neill 2003). The simulations predict the existence of some almost pure core fragments. These will have so little calcium that they are unlikely to be detected and we, therefore, remove from the model population all fragments with core masses higher than $C_f > 0.826$ or Ca/Fe $< 8.9 \times 10^{-3}$, where Ca/Fe $= 8.9 \times 10^{-3}$ is the lowest observed Ca/Fe ratio in any polluted white dwarf in the sample.

We consider that the distribution of core mass fractions produced by the collisional evolution seen in these simulations will be fairly typical of collisional evolution in most planetesimal belts, although the exact details will clearly vary depending on the exact collisional and dynamical history of the individual planetary system.

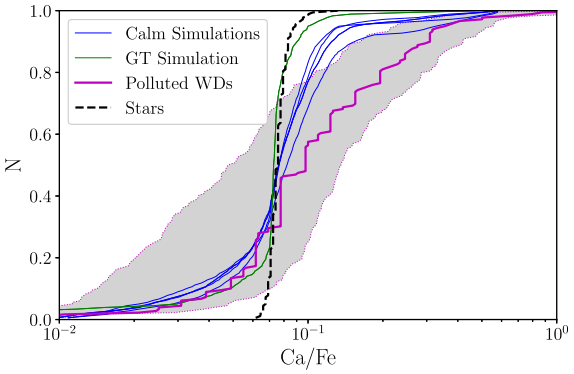

Figure 4. The same as Fig. 2 but now including the cumulative distribution of Ca/Fe abundances predicted from the simulations, the blue solid lines show the *Calm* simulations and the green solid line shows the GT simulations.

5.2 The fraction of exoplanetesimals that are differentiated

Not all bodies that accrete on to white dwarfs will be fragments of differentiated planetesimals. In some planetary systems, small exoplanetesimals may not differentiate and these may be the planetesimals that accrete on to white dwarfs. In our Solar system, some bodies that formed early in the inner system show clear evidence for differentiation (i.e. iron meteorites), while other asteroids remain unaltered, such as the chondritic meteorites. In fact, the exact frequency of differentiated bodies within our asteroid belt remains a subject of debate (DeMeo et al. 2015). In exoplanetary systems, there may not have been a sufficient heat budget to lead to differentiation (e.g. short-lived radioactive nuclides), or planetesimals may have formed too late to take advantage of this. We, therefore, introduce a parameter $f_{\rm diff}$, which represents the fraction of exoplanetesimals accreted by white dwarfs that are fragments of differentiated bodies. We consider this to be a good proxy for the fraction of exoplanetary systems in which planetesimals are differentiate. The model is now defined as

$$k^{\rm diff}(\mathbf{X}_{\rm Ca/Fe}) = f_{\rm diff}\, k^{\rm sims}(\mathbf{X}_{\rm Ca/Fe}) + (1 - f_{\rm diff})\, k^{\rm stars}(\mathbf{X}_{\rm Ca/Fe}), \qquad (4)$$

where $k^{\rm diff}(\mathbf{X_{Ca/Fe}})$ is the cumulative distribution of Ca/Fe ratios predicted by the model, which is found as a sum of the cumulative distribution of Ca/Fe ratios predicted from the simulations, $k^{\rm sims}(\mathbf{X_{Ca/Fe}})$ and the cumulative distribution of Ca/Fe ratios predicted for the initial conditions at the start of planet formation, $k^{\rm stars}(\mathbf{X_{Ca/Fe}})$, which both are a function of the Ca/Fe ratio, $\mathbf{X_{Ca/Fe}}$. A 1D interpolation is used to convert between $k^{\rm diff}(\mathbf{X_{Ca/Fe}})$ and $X^{\rm diff}_{\rm Ca/Fe}(\mathbf{k})$. The MCMC fitting routine (Foreman-Mackey et al. 2013) is used to maximize the likelihood function (equation 2) in order to find the posterior distribution of $f_{\rm diff}$, assuming a uniform prior in which $0 < f_{\rm diff} < 1$. The best-fitting value is very close to 1, with $f_{\rm diff} = 99^{+0.8}_{-1.8}$ per cent averaged over all *Calm* simulations. In other words, the data is consistent with almost all white dwarf pollutants being the fragments of differentiated planetesimals.

Fig. 4 shows the cumulative distribution of Ca/Fe ratios predicted by the model with differentiation, compared to the observed population. The uncertainties in the observed abundances are such that this model is consistent with the observations ($\chi^2 < 2$; equation 1). In fact, such a small χ^2 may be indicative that the errors on the abundances are in some cases overestimated. In most cases, quoted errors are very conservative, taking into account both potential errors on the atomic data and white dwarf atmosphere models.

By comparing the likelihoods (Table 1), we can see that a model in which all planetesimals are differentiated is significantly more likely as an explanation for the data than a model in which the range of Ca/Fe ratios is explained only by the small variation in the initial conditions for planet formation (no exoplanetesimals are differentiated).

However, while the model is a reasonable fit to the observations at low Ca/Fe ratios, it is less successful at high Ca/Fe ratios. The reasons for this will be discussed in detail in the next section; however, we consider those observations with low Ca/Fe ratios (Ca/Fe < 0.07) as a useful sample for better constraining the fraction of planetesimals that are differentiated, $f_{\rm diff}$. Ca/Fe $= 0.07$ is the median of the distribution of Ca/Fe in nearby stars, while also being equivalent to a core mass fraction of $C_{\rm f} = 0.35$, assuming typical parameters for bulk Earth (equation 3). Maximizing the likelihood (equation 2) considering only low Ca/Fe ratios (Ca/Fe < 0.07) finds a posterior distribution of $f_{\rm diff}$ as shown in Fig. 5. While all exoplanetesimals being differentiated ($f_{\rm diff} = 1.0$) remains the most likely model, a good fit to the data is found even when the fraction of exoplanetesimals that are differentiated is as low as 65 per cent.

6 THE OVERABUNDANCE OF POLLUTED WHITE DWARFS WITH HIGH CA/FE RATIOS

There are more polluted white dwarfs with high Ca/Fe ratios in the observed population than in the model population in which all exoplanetesimals are differentiated. This can be seen in Fig. 4, where the third quartile (84 per cent) occurs at Ca/Fe $= 0.1$ for the model population and Ca/Fe $= 0.24$ for the observed population. The model and the observed populations are consistent for low Ca/Fe ratios, but clearly diverge for Ca/Fe ratios above the average. Fig. 6 uses the observed Ca/Fe ratios to predict the core mass fractions of the planetesimals accreted by the white dwarfs, using the inverse of equation (3). This figure clearly shows that the Ca/Fe ratios observed would represent a significant overabundance of mantle-rich fragments compared to the simulated population. Here, we discuss other potential reasons for this divergence.

The observed population is by no means selected in an unbiased manner. The white dwarfs used here have been collated from the literature, where in general the objects with the best determined abundances are published. Even a large number of white dwarfs in Hollands et al. (2017) have not been selected in a uniform manner. Rather, they were identified in SDSS DR 12 due to the presence of sufficient metal lines in the spectra to alter their broad-band magnitudes, such that they have redder $u - g$ colours than the main sequence in a $u - g$ versus $g - r$ colour–colour diagram, rather than bluer like most white dwarfs. In addition to that, only white dwarfs where all three major elements Ca, Fe, and Mg were detected are included.

We can, however, consider the impact that requiring both Ca and Fe are detected might have on the model population. Calcium is easier to detect than iron, yet, present in smaller quantities in planetary material. No calcium will be present in purely core fragments, which have, therefore been removed from the model population as undetectable. Fig. 1 shows that the fragments with low Fe abundances have high Ca/Fe ratios and thus the non-detection of these fragments leads the observational sample to be biased towards low Ca/Fe ratios. This is the opposite trend to that seen in the observations. We, therefore, consider that we do not find strong evidence that observational biases are responsible for the overabundance of high Ca/Fe ratios in the observed population.

Table 1. A table to show the results of comparing the model populations to the white dwarf observations. Best-fitting parameters are shown, alongside reduced chi-squared (equation 1) and likelihoods (equation 2).

Model	χ^2	ln L	$f_{\rm diff}$	$f_{\rm hot}$	$d_{\rm Ca/Fe}$	$\sigma_{\rm w}$
Stars	3.5	−180				
Diff: GT	0.83	230	98.4^{+1}_{-2} per cent			
Diff: Calm1	0.46	300	98.2^{+1}_{-2} per cent			
Diff: Calm2	0.26	330	98.5^{+1}_{-3} per cent			
Diff: Calm3	0.43	300	98.1^{+1}_{-3} per cent			
Diff: Calm4	0.42	305	98.2^{+1}_{-3} per cent			
Hot: GT	0.57	330	69^{+1}_{-1} per cent	30^{+1}_{-1} per cent	0.25 ± 0.01	0.07 ± 0.02
Hot: Calm1	0.13	370	62^{+5}_{-6} per cent	34^{+5}_{-5} per cent	0.23 ± 0.02	0.11 ± 0.03
Hot: Calm2	0.08	374	66^{+8}_{-7} per cent	29^{+6}_{-8} per cent	0.21 ± 0.03	0.11 ± 0.03
Hot: Calm3	0.16	367	67^{+3}_{-3} per cent	31^{+3}_{-3} per cent	0.23 ± 0.02	0.09 ± 0.02
Hot: Calm4	0.09	373	66^{+5}_{-5} per cent	31^{+4}_{-5} per cent	0.23 ± 0.02	0.11 ± 0.03

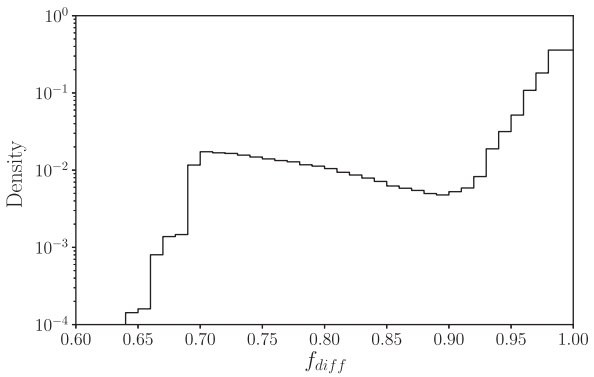

Figure 5. The posterior distribution for the fraction of exoplanetesimals that are differentiated, $f_{\rm diff}$, considering only observations with low Ca/Fe (Ca/Fe < 0.07). While the most likely solution is that almost all exoplanetesimals are differentiated, a good fit to the data can be found with as low as 65 per cent of exoplanetesimals being differentiated.

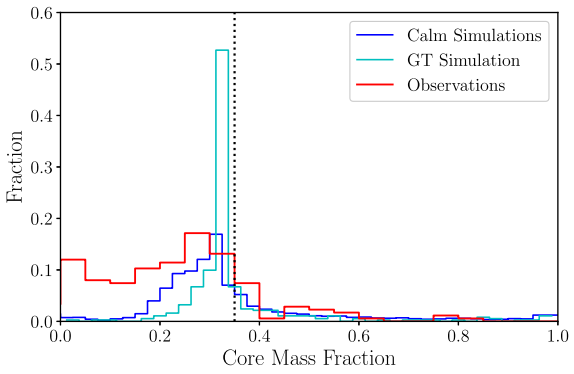

Figure 6. The overabundance of white dwarfs with high Ca/Fe ratios, as discussed in Section 6, is apparent when only the Ca/Fe ratio is used to predict the core mass fractions of the bodies accreted by the white dwarf sample (equation 3), shown in the figure compared to the distribution of core mass fractions from the simulations (see Section 5.1). In Section 6, we discuss alternative explanations to explain the overabundance of apparently core-rich fragments, derived from the overabundance of polluted white dwarfs with high Ca/Fe.

One tendency of the simulations, as discussed in Section 5.1, is to produce more mantle-rich fragments than core-rich fragments. This occurs as many gentle collisions chip off small pieces of mantle. Unfortunately, the simulations are unable to resolve these small fragments and therefore, they are assumed to reaccrete on to all fragments uniformly. This leads to many fragments with core fractions slightly below average. However, if these fragments could be followed in detail, or if collisions were more violent, such as that may occur in a system stirred by giant planets, it is plausible that the distribution of core mass fractions may be skewed to contain more very mantle-rich fragments. Such fragments would produce a model population that tends to have more mantle-rich fragments and be more similar to that predicted from the observations; however, there will still be many more moderately mantle-rich fragments than extremely mantle-rich fragments. Fig. 6 indicates how extreme this overabundance of high Ca/Fe ratios in the observed population is compared to the simulations, which makes it hard to explain with this model. The observations were sensitive enough to detect white dwarfs with low Ca/Fe ratios, as demonstrated by a handful of extreme examples, but these were found to be rare in Hollands et al. (2017).

The simulations assume a single initial Ca/Fe ratio of Ca/Fe = 0.07 ($C_{\rm f} = 0.35$) for all planetesimals. A range of initial Ca/Fe may be more appropriate across diverse exoplanetary systems, and indeed a range of Ca/Fe ratios are seen across chondritic meteorites in our Solar system (0.04–0.11; Wasson & Kallemeyn 1988), although some of the spread may be due to the effects of heating]. We do not deem a range in the initial Ca/Fe as a likely explanation for the observed overabundance, as a large spread towards high Ca/Fe would be required.

The collision model did not include crustal differentiation. This has the potential to increase the number of fragments with high calcium abundances (Carter et al. 2018). Crustal stripping is particularly efficient at producing small fragments with high Ca/Fe ratios. Such fragments would also have altered abundances of other species. In addition to this, crustal material is generally a significantly smaller proportion of a planetary body's overall mass budget (e.g. <0.5 per cent for Earth) and even when it is taken into account that smaller planetesimals may have deeper crusts, like Vesta, it is hard to envisage that crustal material accounts for such a large fraction of the population.

Processes related to heating at temperatures higher than 1000 K can, on the other hand, increase the Ca/Fe ratio of planetary bodies. Ca is more refractory than iron, with a 50 per cent condensation temperature of 1660 K compared to 1357 K (Lodders 2003). This means that at typical temperatures occurring in the inner regions of protoplanetary discs, grains that condensed at temperatures between around 1000 and 2000 K could contain more calcium-

rich minerals than iron-rich minerals. Alternatively, heating during the star's evolution on the giant branch could heat material to similar temperatures, leading to the removal of more iron-rich minerals. Such processes can only enhance, and not deplete, the Ca/Fe ratio of solids. We, therefore, propose that heating could lead to the overabundance of planetesimals with high Ca/Fe ratios accreted by white dwarfs, in a similar manner to Harrison, Bonsor & Madhusudhan (2018), and assess the validity of this model in the next section.

6.1 High temperatures lead to an increase in Ca/Fe

In this section, we investigate whether a model in which some planetesimals accreted by white dwarfs have higher Ca/Fe ratios due to the effects of heat processing can explain the white dwarf observations. The increased Ca/Fe ratio could have occurred due to incomplete condensation of iron-rich minerals during planet formation, or evaporation during formation or subsequent evolution, for example on the giant branch. The exact distribution of Ca/Fe is, thus, unknown. There is an additional complication that heating and differentiation can occur in the same planetesimals. We, therefore, decide not to focus on producing a detailed model of heating, but make a broad, all-encompassing model that can tell us whether this explanation has the potential to be consistent with the population. We, therefore, parametrize the distribution of Ca/Fe ratios due to heating as a normal distribution centred at $d_{\rm Ca/Fe}$, of width $\sigma_{\rm W}$, where both $d_{\rm Ca/Fe}$ and $\sigma_{\rm W}$ are model parameters. Clearly, such a model is sufficiently flexible to fit the observations, given appropriate values of $d_{\rm Ca/Fe}$ and $\sigma_{\rm W}$; however, it can provide an indication of the fraction of the population for which heating is important.

We create a model in which a fraction, $f_{\rm hot}$, of the sample has undergone heating that leads to a cumulative distribution of Ca/Fe abundances, $k^{\rm hot}(\mathbf{X_{Ca/Fe}})$, given by the cumulative distribution function of a Gaussian centred on $d_{\rm Ca/Fe}$ and of width σ. At the same time, we consider that a fraction, $f_{\rm diff}$, of the sample are fragments of differentiated planetesimals, with a distribution of abundances that follow those of the simulations, $k^{\rm sims}(\mathbf{X_{Ca/Fe}})$. Those white dwarf pollutants that are not differentiated, nor have experienced heating ($1 - f_{\rm diff} - f_{\rm hot}$), have abundances that originate from the distribution of potential initial abundances, i.e. from nearby stars, $k^{\rm stars}(\mathbf{X_{Ca/Fe}})$. This leads to a model with four free parameters: $f_{\rm diff}$, $f_{\rm hot}$, $d_{\rm Ca/Fe}$, and $\sigma_{\rm W}$. We use this to calculate the model population, where $k^{\rm model}(\mathbf{X_{Ca/Fe}})$ is the cumulative distribution of Ca/Fe ratios in the model population, where

$$k^{\rm model}(\mathbf{X}_{\rm Ca/Fe}) = f_{\rm diff}\, k^{\rm sims}(\mathbf{X}_{\rm Ca/Fe}) + (1 - f_{\rm diff} - f_{\rm hot})\, k^{\rm stars}(\mathbf{X}_{\rm Ca/Fe}) + f_{\rm hot}\, k^{\rm hot}(\mathbf{X}_{\rm Ca/Fe}). \quad (5)$$

We find the best-fitting values of $f_{\rm diff}$, $f_{\rm hot}$, $d_{\rm Ca/Fe}$, and $\sigma_{\rm W}$ by maximizing the posterior distribution (equation 2) using the MCMC fitting routine of Foreman-Mackey et al. (2013) and assuming uniform priors of $0 < f_{\rm diff} < 1$, $0 < f_{\rm hot} < 1$, $0.07 < d_{\rm Ca/Fe} < 0.4$, and $0 < \sigma_{\rm W} < 0.3$. The mid-point of the Gaussian is fixed to occur at high Ca/Fe ratios, i.e. above Ca/Fe = 0.07, equivalent to $C_{\rm f} = 0.35$; otherwise the priors are designed to be non-informative and encompass the full range of potential values for the parameters.

The results of the fitting procedure are listed in Table 1, while the posterior probability distributions of the four parameters are shown in Fig. 7. Fig. 7 plots all 50 walkers at steps 1000 to 2000, in the four *Calm* simulations, with contours overlaid at (0.1, 0.5, 1.0, 1.5, 2.0)σ. The distributions show the existence of a clear best-fitting solution.

Fig. 7 shows there is a correlation between $f_{\rm diff}$ and $f_{\rm hot}$. Those models in which more exoplanetesimals are differentiated ($f_{\rm diff}$ is higher) show less effects of heating ($f_{\rm hot}$ is lower). This naturally makes sense as both parameters help to explain the excess of polluted white dwarfs with high Ca/Fe ratios. However, solutions for $f_{\rm diff}$ and $f_{\rm hot}$ all lie within the defined ranges, with best-fitting values of 66^{+4}_{-6} per cent for $f_{\rm diff}$ and $f_{\rm hot} = 31^{+5}_{-5}$ per cent, averaged across all *Calm* simulations. The fraction of planetesimals that are differentiated is in-line with the model that focused only on low Ca/Fe ratios (Section 5.2), the difference here being that a model in which all exoplanetesimals are differentiated is no longer such a good model for the data, which instead favours a significant fraction of exoplanetesimals to be influenced by the effects of heating. This model is shown as the red solid line on Fig. 8.

For the heating model best-fitting values of $d_{\rm Ca/Fe} = 0.23^{+0.03}_{-0.03}$, $\sigma_{\rm w} = 0.1^{+0.03}_{-0.03}$ per cent, averaged across all *Calm* simulations. In terms of the mid-point ($d_{\rm Ca/Fe}$) and width (σ_w) of the Gaussian, the majority of solutions indicate the addition of planetesimals with Ca/Fe ratios between 0.1 and 0.3 due to heating. These are very plausible values for objects where some iron-rich minerals have been removed and the Ca/Fe ratio was fixed prior to differentiation. Such high Ca/Fe ratios are less likely to occur following differentiation, as they would require the removal of more iron than generally found in the body's mantle.

7 DISCUSSION

In this work, we present a model in which the population of calcium and iron abundances observed in a sample of 179 polluted white dwarfs can be explained by the differentiation and collisional processing of a substantial fraction of the accreted planetesimals and the effects of processing at temperatures higher than 1350 K. We aim to constrain how frequently planetesimals accreted by white dwarfs are the collision fragments of differentiated bodies. In this section, we discuss how robustly we can come to a conclusion.

Our null hypothesis was that the range of abundances observed in the planetary bodies accreted by white dwarfs resulted from a range of initial abundances present in the material out of which the planetary bodies formed. Using nearby stars as a proxy for this range of compositions, we show that this model is unlikely to explain the data. We deem it likely that differentiation, rather than other unknown processes, is responsible for the abundances in at least some white dwarfs due to the correlations observed in multiple siderophile species (core) or multiple lithophile species (mantle), which point towards segregation due to melting and differentiation (Jura & Young 2014; Harrison et al. 2018). In fact, those polluted white dwarfs in this sample with the lowest Ca/Fe ratios also have the lowest Mg/Fe ratios, pointing towards a common origin to the depletion of both lithophiles (Hollands et al. 2018). In a similar manner, correlations between the abundances of multiple species linked by similar condensation temperatures provide evidence for heat processing in individual objects (Harrison et al. 2018).

A model in which all white dwarf pollutants are fragments of differentiated bodies is consistent with the data, given the uncertainties. However, an excess of high Ca/Fe ratios in the observed sample compared to the model remains. We hypothesize that this excess can be explained by planetesimals that have suffered the effects of heat processing at temperatures between 1000 and 2000 K. At such temperatures, calcium-rich and iron-rich minerals exhibit different behaviours, with iron-rich minerals tending to be removed preferentially from the solid phase compared to calcium-rich minerals, which can lead to high Ca/Fe ratios in

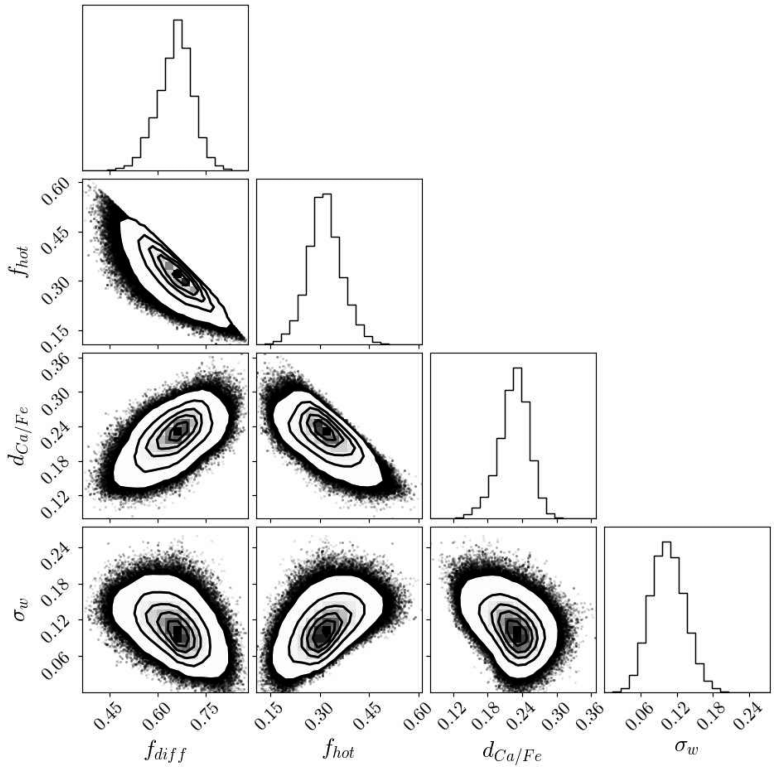

Figure 7. The posterior probability distributions of each parameter in the empirical fit to observations, calculated by maximizing the likelihood (equation 5), assuming that a fraction $f_{\rm diff}$ of planetesimals is differentiated, while $f_{\rm hot}$ are subject to heating. Results are included for four high-resolution *Calm* simulations. Plotted are individual walkers, with density contours overplotted at (0.1, 0.5, 1.0, 1.5, 2.0)σ, created using Foreman-Mackey (2016).

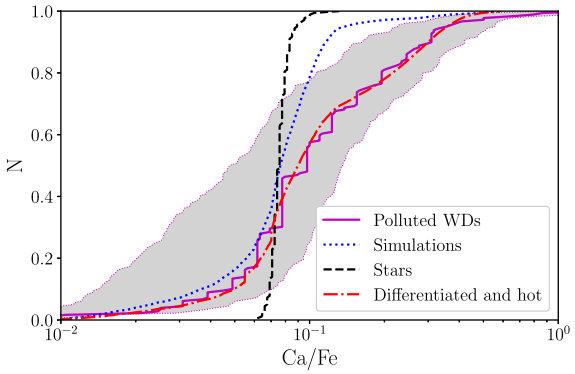

Figure 8. The same as Fig. 2 but now including the cumulative distribution of Ca/Fe abundances predicted from the model with both heating and differentiation (red dot–dashed line), compared to the blue dotted line that shows the *Calm 1* simulation. $f_{\rm hot} = 31$ per cent, $f_{\rm diff} = 66$ per cent, $d_{\rm Ca/Fe} = 0.24$, and $\sigma_{\rm W} = 0.09$.

planetary bodies. We know from the Solar system that the effects of the depletion of moderately volatile elements, including trends featuring Ca and Fe, are seen in meteoritic samples (e.g. Palme & O'Neill 2003). It, therefore, seems probable that such processes would have occurred in the planetesimals accreted by white dwarfs, long prior to their accretion on to the white dwarfs.

The key question is regarding the fraction of exoplanetesimals that are differentiated. Based on the model analysis, we consider that between 60 and 100 per cent of exoplanetesimals are differentiated, with a most likely value of 66^{+4}_{-6} per cent. The best way to improve upon these conclusions would be to increase the sample size, particularly the sample size of white dwarfs with precisely determined abundances of at least Ca and Fe. For example, there are less than 10 white dwarfs with low Ca/Fe (<0.07) and high S/N (>10) from which the most can be learnt about the fraction of planetesimals that are differentiated. This is not yet large enough to smooth out the effects of small number statistics.

7.1 Limitations of the model

The current model suffers from many limitations, which will be discussed here. However, we note that the limitations of the model must be considered in the context of the size of the data sample with sufficiently precise abundance determinations and our lack of knowledge regarding any biases in its selection. The most significant weakness of this work is that we focus solely on Ca and Fe. While this allows us to process a larger data sample in the same manner, we are not taking advantage of the full information available for each white dwarf. Ca and Fe are a very useful pair of elements as the effects of differential sinking in the white dwarf atmosphere can be ignored. Conclusions regarding individual objects will be found in Harrison et al. in preparation.

The model is relatively simplistic. We create a model of collision fragments based on the collisional history of a single planetary system. While the white dwarf pollutants necessarily originate from a wide range of systems, it is not feasible to simulate even a small range of the potential architectures. We do, however, predict that the range of core mass fractions produced will vary in width and height, rather than significantly in form. We hypothesize that the generic form, whereby collisional evolution produces a centrally peaked distribution of Ca/Fe ratios, or indeed core mass fractions,

with fewer fragments possessing extreme values, will be consistent across a wide range of system architectures.

The main conclusions of this work are based on the existence of many more bodies with Ca/Fe (core mass fractions) close to a central (original) value than extreme values. In fact, the fraction of exoplanetesimals that must be differentiated would only increase if the distribution were more centrally peaked, a plausible consequence of more dramatic collisional evolution, as seen in the GT simulation (see Fig. 3). If the distribution of Ca/Fe ratios were spread more broadly in systems with particular collision histories, it is plausible that the fraction of exoplanetesimals that are differentiated has been overestimated. However, the number of white dwarf pollutants with extreme Ca/Fe ratios limits any potential reduction.

We sample the Ca/Fe ratios produced in a single planetary system at a single epoch. We can consider this to be a reasonable approximation to the collisional evolution at larger orbital radii on longer time-scales, as discussed in Section 5. However, necessarily we cannot sample a full range of systems at a full range of applicable epochs. We can, however, justify the sampling of a single system at a single epoch, as the collisional evolution tends after a period of initial evolution to a relatively steady distribution of Ca/Fe in the bodies considered. This means that if the white dwarf pollutants sample systems at a range of orbital radii, we anticipate that the distribution in Ca/Fe may not depend strongly on orbital radii, for those systems where collisional equilibrium is established. This does, however, require further detailed investigation.

We assume that each white dwarf has accreted a single fragment. If instead multiple fragments were important, this could potentially act to smooth the distribution of Ca/Fe ratios (Turner & Wyatt 2019) and we would expect to see fewer examples of white dwarf pollutants with extreme abundances. This would make it harder to conclude that any white dwarf pollutants are not the fragments of differentiated exoplanetesimals. It is, however, potentially possible that white dwarfs accrete differentiated bodies in a biased manner, for example accreting first material from the mantle, followed by material from the core.

We ignore crustal fragments, which do have the potential to alter the Ca/Fe ratio. This would likely mean that some pollutants with high Ca/Fe may result from crustal fragments, rather than heating, thus reducing $f_{\rm hot}$, while leaving $f_{\rm diff}$ unaffected. This is an important avenue for future investigations.

The heating model is very simplistic and presented merely to show that heating is a plausible explanation for the overabundance of white dwarfs with high Ca/Fe ratios, rather than as a precise distribution of the Ca/Fe ratios likely to exist in planetesimals following the effects of temperatures higher than 1000 K. We refer the interested reader to Harrison et al. (2018) for a more detailed description of the Ca/Fe ratios that may result from the effects of heating on exoplanetesimals.

7.2 The implications of the results for exoplanetary systems

We have shown that many white dwarf pollutants are likely to be the collision fragments of planetesimals that differentiated to form a core and a mantle. The implications of this conclusion depends on the size of planetesimals that are accreting on to white dwarfs, which remains an open question. While we can measure the mass of material currently in the atmosphere of the white dwarf, which in some cases is greater than the mass of Ceres (Raddi et al. 2015), exactly how this relates to the size of the body accreted, or the size of the parent body, if the pollutant is a collision fragment, remains unclear.

If the white dwarf pollutants are the collision fragments of parent bodies larger than around >1000 km in diameter, their differentiation can be explained by the heating imparted by impacts occurring during planet formation (Davison et al. 2010). This would imply that a large proportion of exoplanetary systems include collisionally evolved populations of Pluto-sized bodies, something which does not seem to be the case within our own Solar system, for example where $D > 100$ km bodies in the asteroid belt are mostly primordial (e.g. Bottke et al. 2015). However, white dwarf planetary systems have the potential for dynamical instabilities to have occurred due to mass-loss post-main sequence (e.g. Veras et al. 2013; Mustill, Veras & Villaver 2014).

On the other hand, the planetesimals accreted by white dwarfs could in general be collisional fragments of bodies smaller than 1000 km. In this case, it is harder to understand what powers their differentiation unless there is a significant source of heating present from short-lived radioactive nuclides in most exoplanetesimals, as suggested by Jura et al. (2013) and Young (2014). Such a theory would support a model in which the presence of these nuclides leads to triggered star formation, such that all planetary systems initially have a large budget of such nuclides (e.g. Boss et al. 2008; Li, Frank & Blackman 2014). In addition to that, it would imply that most white dwarf pollutants originate from sufficiently close to the star that planetesimal growth had made it to large enough sizes to differentiate prior to the decay of any short-lived radioactive nuclides present in the planet-forming material, e.g. ^{26}Al with its half life of 0.7 Myr.

The requirement for the collisional evolution of large planetesimals, whether they are of the order of $\sim$10 km in size, or much larger, in most white dwarf planetary systems implies that most of these systems possess debris belts significantly more massive than our own Solar system's asteroid or Kuiper belt. This agrees with observations of main-sequence debris discs, which find that, for example, $\sim$ 30 per cent of main-sequence A stars have a debris belt detectable with *Spitzer* (Su et al. 2006; Wyatt 2008), while our asteroid and Kuiper belt lie orders of magnitude below the detection limit. Another possibility is that the dynamical instabilities that lead to white dwarf pollution (e.g. Debes & Sigurdsson 2002; Bonsor et al. 2011; Debes et al. 2012) lead to collisional processing in large bodies. The most likely scenario is that in some systems, the white dwarf pollutants result from the collisional processing of very large bodies (>1000 km) that are differentiated, while in other systems, the presence of short-lived radioactive nuclides leads to the differentiation of smaller bodies.

We have also shown that heat processing above 1350 K of some material in about a third of the white dwarf pollutants can explain their Ca and Fe abundances. Such temperatures are only reached during planet formation interior to 1.5 au in a Chambers (2009) protosolar nebula (Harrison et al. 2018). On the other hand, heating during the giant branch evolution suggests that a 3 $M_\odot$ star can reach a luminosity of 16 000 $L_\odot$ at the tip of the AGB (Hurley, Pols & Tout 2000), which would imply an equilibrium temperature of >1350 K for bodies interior to 6 au. If this explanation for the Ca/Fe abundances is correct, this implies that about a third of white dwarf pollutants originate from planetesimal belts within a few au of their host stars. There is clear evidence that some white dwarf pollutants that have retained volatiles such as water originated from planetesimal belts outside of the ice line (Farihi et al. 2011; Raddi et al. 2015; Malamud & Perets 2016). Thus, in combination with the need for heating, white dwarf abundances imply that a large spread in the original radii of white dwarf pollutants must exist.

8 CONCLUSIONS

Abundances of calcium and iron in the atmospheres of white dwarfs can be used to study the differentiation of exoplanetesimals. We use a sample of 179 white dwarfs collated from the literature, where both Ca and Fe are detected, to show that the distribution of Ca/Fe ratios are unlikely to occur as a result of a distribution in the initial compositions (Ca/Fe) at the start of planet formation. We hypothesize that, instead, a fraction of the white dwarfs have accreted the fragments of differentiated exoplanetesimals.

If exoplanetesimals differentiate, collisions can lead to fragments with a range of core mass fractions (Ca/Fe). We present results from a set of *N*-body simulations in which the fate of core and mantle material during collisions is traced separately. These simulations show that the distribution of core mass fractions in the remnant planetesimals is always dominated by values close to the core mass fraction of the parent bodies, with a few extremely core-rich or mantle-rich fragments. This means that while it is easy to conclude that white dwarf pollutants with extreme Ca/Fe ratios are likely to be core-rich or mantle-rich fragments, for every extreme observation, we anticipate many more white dwarf pollutants with less extreme Ca/Fe ratios.

Using the simulation results, we created a model population of planetesimals that could accrete on to polluted white dwarfs. We use this model to show that the observed range of Ca/Fe ratios in polluted white dwarfs is consistent with all polluted white dwarfs having accreted the collision fragment of a differentiated planetesimal; however, there is an overabundance of polluted white dwarfs observed with high Ca/Fe ratios. We suggest that this is unlikely to be an observational bias and more likely a result of processing at temperatures between 1000 and 2000 K during the formation or subsequent evolution of the accreted planetesimals. In this case, our best-fitting model finds that 31^{+5}_{-5} per cent of planetesimals accreted by white dwarfs have increased Ca/Fe due to the effects of heating, while 66^{+4}_{-6} per cent are the fragments of differentiated planetesimals.

These results imply that the collisional evolution of large planetesimals (at least larger than tens of kilometres) is a typical feature of exoplanetary systems, in line with observations of debris discs around main-sequence stars. The population of white dwarf pollutants suggests that differentiation occurs commonly in exoplanetesimals and that either short-lived radioactive nuclides are present in many exoplanetary systems, or white dwarf pollutants are typically the collision remnants of planetary bodies sufficiently large that impacts during planet formation can lead to differentiation. We highlight the need for a larger sample of white dwarfs with precisely determined abundances to investigate further the geological process of differentiation in exoplanetary systems.

ACKNOWLEDGEMENTS

AB acknowledges funding from a Royal Society Dorothy Hodgkin Fellowship. JHDH acknowledges an STFC studentship. BTG was supported by the UK STFC grant ST/P000495. PJC acknowledges support from UC Office of the President grant LFR-17-449059. The research leading to these results has received funding from the European Research Council under the European Union's Horizon 2020 research and innovation programme no. 677706 (WD3D). AB acknowledges funding from a Royal Society Dorothy Hodgkin Fellowship (DH150130).

REFERENCES

Bauer E. B., Bildsten L., 2018, ApJ, 859, L19
Bauer E. B., Bildsten L., 2019, ApJ, 872, 96
Benz W., Slattery W. L., Cameron A. G. W., 1988, Icarus, 74, 516
Bonsor A., Mustill A. J., Wyatt M. C., 2011, MNRAS, 414, 930
Bonsor A., Leinhardt Z. M., Carter P. J., Elliott T., Walter M. J., Stewart S. T., 2015, Icarus, 247, 291
Boss A. P., Keiser S. A., 2010, ApJ, 717, L1
Boss A. P., Ipatov S. I., Keiser S. A., Myhill E. A., Vanhala H. A. T., 2008, ApJ, 686, L119
Bottke W. F., Brož M., O'Brien D. P., Campo Bagatin A., Morbidelli A., Marchi S., 2015, in Patrick M., Francesca E. D., William F. B., eds, Asteroids IV. Univ. Arizona Press, Tucson, p. 701
Brewer J. M., Fischer D. A., Valenti J. A., Piskunov N., 2016, ApJS, 225, 32
Burbine T. H., McCoy T. J., Meibom A., Gladman B., Keil K., 2002, Asteroids III. Arizona Univ. Press, Tucson, p. 653
Carter P. J., Leinhardt Z. M., Elliott T., Walter M. J., Stewart S. T., 2015, ApJ, 813, 72
Carter P. J., Leinhardt Z. M., Elliott T., Stewart S. T., Walter M. J., 2018, Earth Planet. Sci. Lett., 484, 276
Chambers J. E., 2009, ApJ, 705, 1206
Cunningham T., Tremblay P.-E., Freytag B., Ludwig H.-G., Koester D., 2019, MNRAS, 488, 2503
Davison T. M., Collins G. S., Ciesla F. J., 2010, Icarus, 208, 468
Deal M., Deheuvels S., Vauclair G., Vauclair S., Wachlin F. C., 2013, A&A, 557, L12
Debes J. H., Sigurdsson S., 2002, ApJ, 572, 556
Debes J. H., Walsh K. J., Stark C., 2012, ApJ, 747, 148
DeMeo F. E., Alexander C. M. O., Walsh K. J., Chapman C. R., Binzel R. P., 2015, Asteroids IV. Arizona Univ. Press, Tucson, p. 13
Dufour P., Kilic M., Fontaine G., Bergeron P., Melis C., Bochanski J., 2012, ApJ, 749, 6
Elkins-Tanton L. T., Weiss B. P., Zuber M. T., 2011, Earth Planet. Sci. Lett., 305, 1
Farihi J., 2016, New Astron. Rev., 71, 9
Farihi J., Brinkworth C. S., Gänsicke B. T., Marsh T. R., Girven J., Hoard D. W., Klein B., Koester D., 2011, ApJ, 728, L8
Farihi J., Gänsicke B. T., Koester D., 2013, Science, 342, 218
Farihi J., Koester D., Zuckerman B., Vican L., Gänsicke B. T., Smith N., Walth G., Breedt E., 2016, MNRAS, 463, 3186
Fischer R. A., Campbell A. J., Ciesla F. J., 2017, Earth Planet. Sci. Lett., 458, 252
Foreman-Mackey D., 2016, J. Open Source Softw., 1, 24
Foreman-Mackey D., Hogg D. W., Lang D., Goodman J., 2013, PASP, 125, 306
Gänsicke B. T., Koester D., Farihi J., Girven J., Parsons S. G., Breedt E., 2012, MNRAS, 424, 333
Ghosh A., McSween H. Y., 1998, Icarus, 134, 187
Gounelle M., 2015, A&A, 582, A26
Gritschneder M., Lin D. N. C., Murray S. D., Yin Q.-Z., Gong M.-N., 2012, ApJ, 745, 22
Harrison J. H. D., Bonsor A., Madhusudhan N., 2018, MNRAS, 479, 3814
Hollands M. A., Koester D., Alekseev V., Herbert E. L., Gänsicke B. T., 2017, MNRAS, 467, 4970
Hollands M. A., Gänsicke B. T., Koester D., 2018, MNRAS, 477, 93
Hughes A. M., Duchene G., Matthews B., 2018, ARAA, 56, 541
Hurley J. R., Pols O. R., Tout C. A., 2000, MNRAS, 315, 543
Jura M., 2003, ApJ, 584, L91
Jura M., Young E. D., 2014, Ann. Rev. Earth Planet. Sci., 42, 45
Jura M., Xu S., Klein B., Koester D., Zuckerman B., 2012, ApJ, 750, 69
Jura M., Xu S., Young E. D., 2013, ApJ, 775, L41
Kawka A., Vennes S., 2012, A&A, 538, A13
Kawka A., Vennes S., 2016, MNRAS, 458, 325
Kennedy G. M., Wyatt M. C., 2010, MNRAS, 405, 1253
Klein B., Jura M., Koester D., Zuckerman B., 2011, ApJ, 741, 64

Kleine T., Mezger K., Palme H., Scherer E., Münker C., 2005, Geochim. Cosmochim. Acta, 69, 5805
Koester D., 2009, A&A, 498, 517
Koester D., Gänsicke B. T., Farihi J., 2014, A&A, 566, A34
Kruijer T. S., Touboul M., Fischer-G'odde M., Bermingham K. R., Walker R. J., Kleine T., 2014, Science, 344, 1150
Landeau M., Olson P., Deguen R., Hirsh B. H., 2016, Nat. Geosci., 9, 786
Leinhardt Z. M., Dobinson J., Carter P. J., Lines S., 2015, ApJ, 806, 23
Li S., Frank A., Blackman E. G., 2014, MNRAS, 444, 2884
Lichtenberg T., Parker R. J., Meyer M. R., 2016, MNRAS, 462, 3979
Lodders K., 2003, ApJ, 591, 1220
Malamud U., Perets H. B., 2016, ApJ, 832, 160
Marcus R. A., Stewart S. T., Sasselov D., Hernquist L., 2009, ApJ, 700, L118
Marcus R. A., Sasselov D., Hernquist L., Stewart S. T., 2010, ApJ, 712, L73
Morbidelli A., Crida A., 2007, Icarus, 191, 158
Mustill A. J., Wyatt M. C., 2009, MNRAS, 399, 1403
Mustill A. J., Veras D., Villaver E., 2014, MNRAS, 437, 1404
Palme H., O'Neill H. S. C., 2003, in Holland H. D., Turekian K. K., eds, Treatise on Geochemistry. Elsevier, Oxford
Raddi R., Gänsicke B. T., Koester D., Farihi J., Hermes J. J., Scaringi S., Breedt E., Girven J., 2015, MNRAS, 450, 2083
Rubie D. C. et al., 2011, Earth Planet. Sci. Lett., 301, 31
Rubie D. C. et al., 2015, Icarus, 248, 89
Scherstén A., Elliott T., Hawkesworth C., Russell S., Masarik J., 2006, Earth Planet. Sci. Lett., 241, 530
Su K. Y. L. et al., 2006, ApJ, 653, 675
Swan A., Farihi J., Koester D., Hollands M., Parsons S., Cauley P. W., Redfield S., Gaensicke B. T., 2019, MNRAS, 490, 202
Turner S. G. D., Wyatt M. C., 2019, MNRAS, 491, 4672
Urey H. C., 1955, Proc. Natl. Acad. Sci., 41, 127
Veras D., 2016, R. Soc. Open Sci., 3, 150571
Veras D., Mustill A. J., Bonsor A., Wyatt M. C., 2013, MNRAS, 431, 1686
Veras D., Leinhardt Z. M., Bonsor A., Gänsicke B. T., 2014, MNRAS, 445, 2244
Wachlin F. C., Vauclair G., Vauclair S., Althaus L. G., 2017, A&A, 601, A13
Wasson J. T., Kallemeyn G. W., 1988, Phil. Trans. R. Soc. A, 325, 535
Wilson D. J., Gänsicke B. T., Koester D., Toloza O., Pala A. F., Breedt E., Parsons S. G., 2015, MNRAS, 451, 3237
Wyatt M. C., 2008, ARA&A, 46, 339
Wyatt M. C., Smith R., Su K. Y. L., Rieke G. H., Greaves J. S., Beichman C. A., Bryden G., 2007, ApJ, 663, 365
Xu S., Jura M., Klein B., Koester D., Zuckerman B., 2013, ApJ, 766, 132
Xu S., Jura M., Koester D., Klein B., Zuckerman B., 2014, ApJ, 783, 79
Xu S., Zuckerman B., Dufour P., Young E. D., Klein B., Jura M., 2017, ApJ, 836, L7
Young E. D., 2014, Earth Planet. Sci. Lett., 392, 16
Zemskova V., Garaud P., Deal M., Vauclair S., 2014, ApJ, 795, 118
Zuckerman B., Koester D., Reid I. N., Hünsch M., 2003, ApJ, 596, 477
Zuckerman B., Melis C., Klein B., Koester D., Jura M., 2010, ApJ, 722, 725
Zuckerman B., Koester D., Dufour P., Melis C., Klein B., Jura M., 2011, ApJ, 739, 101

APPENDIX A

Table A1. The sample of polluted white dwarfs where both calcium and iron were detected, as used in this work.

Name	$T_{\rm eff}$ K	Ca/H(e) dex	$\sigma_{\rm Ca}$ dex	Fe/H(e) dex	$\sigma_{\rm Fe}$ dex	Ca/Fe	$\sigma_{\rm Ca/Fe}$
WD0122−227*	8380	−10.10	0.10	−8.5	0.20	0.03	0.01
WD0446−255*	10 120	−7.40	0.10	−6.9	0.10	0.32	0.10
WD0449−259*	9850	−9.10	0.10	−7.9	0.20	0.06	0.03
WD1350−162*	11 640	−8.70	0.10	−7.1	0.10	0.03	0.01
WD2105−820*	10 890	−8.20	0.10	−6.0	0.20	0.01	0.00
WD2115−560*	9600	−7.40	0.10	−6.4	0.10	0.10	0.03
WD2157−574*	7010	−8.10	0.10	−7.3	0.10	0.16	0.05
WD2216−657*	9190	−9.00	0.10	−8.0	0.20	0.10	0.05
GD 40[α]	15 300.0	−6.90	0.20	−6.47	0.12	0.37	0.20
GD 61[β]	17 300.0	−7.90	0.06	−7.6	0.07	0.50	0.11
SDSS J0738+1835[γ]	14 000.0	−6.23	0.15	−4.98	0.09	0.06	0.02
PG 1225−079[ϵη]	10 800.0	−8.06	0.03	−7.42	0.07	0.23	0.04
GD 362[ϵ]	10 500.0	−6.24	0.10	−5.65	0.10	0.26	0.08
G241−6[ζ]	15 300.0	−7.30	0.20	−6.82	0.14	0.33	0.19
HS 2253+8023[η]	14 400.0	−6.99	0.03	−6.17	0.03	0.15	0.01
SDSS J124231+522627[θ]	13 000.0	−6.53	0.10	−5.9	0.15	0.23	0.10
WD 1536+520[ι]	20 800.0	−5.28	0.15	−4.5	0.15	0.17	0.08
SDSS J0845+2257[κλ]	19 780.0	−5.95	0.10	−4.6	0.20	0.04	0.02
PG 1015+161[λ]	19200.0	−6.45	0.20	−5.5	0.30	0.11	0.09
SDSS 1228+1040[λ]	20 900.0	−5.94	0.20	−5.2	0.30	0.18	0.15
GALEX 1931+0117[λ]	21 200.0	−6.11	0.04	−4.5	0.30	0.02	0.02
G149−28[ζ]	6020.0	−8.04	0.16	−7.41	0.15	0.23	0.12
G29−38[ρ]	11 800.0	−6.58	0.12	−5.9	0.10	0.21	0.08
NLTT 43806[ζ]	5900.0	−7.90	0.19	−7.8	0.17	0.79	0.47
SDSS J0002+3209[†]	6410.0	−9.05	0.18	−7.84	0.18	0.06	0.04
SDSS J0006+0520[†]	6790.0	−9.00	0.16	−8.39	0.16	0.25	0.13
SDSS J0010−0430[†]	6960.0	−8.38	0.15	−7.12	0.15	0.05	0.03
SDSS J0019+2209[†]	5970.0	−9.34	0.16	−8.58	0.16	0.17	0.09
SDSS J0044+0418[†]	6050.0	−9.82	0.08	−8.71	0.08	0.08	0.02
SDSS J0046+2717[†]	7640.0	−7.65	0.24	−6.84	0.24	0.15	0.12

Table A1 *– continued*

Name	$T_{\rm eff}$ K	Ca/H(e) dex	$\sigma_{\rm Ca}$ dex	Fe/H(e) dex	$\sigma_{\rm Fe}$ dex	Ca/Fe	$\sigma_{\rm Ca/Fe}$
SDSS J0047+1628†	6620.0	− 7.68	0.18	− 6.47	0.18	0.06	0.04
SDSS J0108−0537†	6010.0	− 8.79	0.14	− 8.08	0.14	0.19	0.09
SDSS J0114+3505†	6370.0	− 8.51	0.21	− 7.2	0.21	0.05	0.03
SDSS J0116+2050†	6207.0	− 8.81	0.08	− 7.6	0.08	0.06	0.02
SDSS J0117+0021†	6800.0	− 8.80	0.08	− 7.6	0.08	0.06	0.02
SDSS J0126+2534†	5320.0	− 9.95	0.14	− 8.64	0.14	0.05	0.02
SDSS J0135+1302†	5800.0	− 9.50	0.11	− 8.69	0.11	0.15	0.06
SDSS J0143+0113†	6700.0	− 8.50	0.08	− 7.3	0.08	0.06	0.02
SDSS J0144+1920†	6500.0	− 8.50	0.18	− 7.39	0.18	0.08	0.05
SDSS J0148−0112†	6830.0	− 8.82	0.20	− 7.31	0.20	0.03	0.02
SDSS J0150+1354†	6310.0	− 7.75	0.17	− 7.24	0.17	0.31	0.17
SDSS J0158−0942†	5940.0	− 9.52	0.18	− 8.41	0.18	0.08	0.04
SDSS J0201+2015†	6180.0	− 8.96	0.14	− 8.25	0.14	0.19	0.09
SDSS J0252−0401†	6950.0	− 8.57	0.14	− 7.46	0.14	0.08	0.04
SDSS J0252+0054†	7500.0	− 8.35	0.16	− 7.14	0.16	0.06	0.03
SDSS J0447+1124†	6530.0	− 8.77	0.19	− 8.06	0.19	0.19	0.12
SDSS J0512−0505†	5563.0	− 8.99	0.06	− 7.79	0.06	0.06	0.01
SDSS J0721+3928†	6280.0	− 8.90	0.15	− 8.09	0.15	0.15	0.08
SDSS J0736+4118†	5100.0	− 8.50	0.12	− 7.69	0.12	0.15	0.06
SDSS J0741+3146†	5592.0	− 9.55	0.16	− 7.5	0.16	0.01	0.00
SDSS J0744+1640†	4940.0	− 10.24	0.24	− 9.33	0.24	0.12	0.10
SDSS J0744+2701†	7890.0	− 7.68	0.17	− 6.87	0.17	0.15	0.08
SDSS J0744+4408†	6370.0	− 8.75	0.23	− 7.54	0.23	0.06	0.05
SDSS J0744+4649†	5028.0	− 8.36	0.08	− 8.17	0.08	0.65	0.16
SDSS J0806+3055†	6900.0	− 7.77	0.23	− 7.16	0.23	0.25	0.19
SDSS J0806+4058†	6808.0	− 8.49	0.08	− 7.49	0.08	0.10	0.03
SDSS J0816+2330†	7790.0	− 7.48	0.24	− 6.37	0.24	0.08	0.06
SDSS J0818+1247†	6810.0	− 8.58	0.25	− 7.77	0.25	0.15	0.13
SDSS J0823+0546†	6019.0	− 9.34	0.06	− 7.36	0.06	0.01	0.00
SDSS J0830−0319†	6400.0	− 9.10	0.11	− 8.29	0.11	0.15	0.05
SDSS J0838+2322†	5670.0	− 9.80	0.09	− 9.3	0.09	0.32	0.09
SDSS J0842+1406†	7160.0	− 8.16	0.08	− 7.3	0.08	0.14	0.04
SDSS J0842+1536†	6180.0	− 9.47	0.22	− 8.46	0.22	0.10	0.07
SDSS J0843+5614†	6600.0	− 8.65	0.16	− 7.74	0.16	0.12	0.07
SDSS J0851+1543†	6300.0	− 8.50	0.09	− 8.2	0.09	0.50	0.14
SDSS J0852+3402†	5580.0	− 9.00	0.20	− 7.79	0.20	0.06	0.04
SDSS J0901+0752†	7100.0	− 7.12	0.11	− 6.21	0.11	0.12	0.04
SDSS J0902+1004†	7250.0	− 8.25	0.22	− 8.19	0.22	0.87	0.63
SDSS J0906+1141†	6910.0	− 7.90	0.25	− 6.94	0.25	0.11	0.09
SDSS J0908+5136†	6180.0	− 9.35	0.10	− 8.24	0.10	0.08	0.02
SDSS J0913+2627†	5210.0	− 9.75	0.21	− 8.64	0.21	0.08	0.05
SDSS J0916+2540†	5378.0	− 7.48	0.08	− 7.09	0.08	0.41	0.10
SDSS J0924+4301†	5950.0	− 9.75	0.26	− 8.54	0.26	0.06	0.05
SDSS J0925+3130†	5810.0	− 9.00	0.10	− 7.99	0.10	0.10	0.03
SDSS J0929+4247†	6530.0	− 8.46	0.16	− 7.15	0.16	0.05	0.03
SDSS J0937+5228†	6600.0	− 8.40	0.09	− 7.5	0.09	0.13	0.04
SDSS J0939+4136†	6310.0	− 8.30	0.18	− 6.79	0.18	0.03	0.02
SDSS J0939+5019†	5980.0	− 8.25	0.20	− 7.14	0.20	0.08	0.05
SDSS J0948+3008†	6000.0	− 9.15	0.14	− 8.44	0.14	0.19	0.09
SDSS J0956+5912†	8800.0	− 7.15	0.09	− 6.14	0.09	0.10	0.03
SDSS J1006+1752†	5710.0	− 9.45	0.21	− 8.34	0.21	0.08	0.05
SDSS J1017+2419†	7200.0	− 8.07	0.13	− 6.96	0.13	0.08	0.03
SDSS J1017+3447†	6150.0	− 9.34	0.19	− 8.33	0.19	0.10	0.06
SDSS J1019+2045†	5300.0	− 9.36	0.26	− 8.25	0.26	0.08	0.07
SDSS J1024+4531†	5980.0	− 8.92	0.17	− 8.11	0.17	0.15	0.09
SDSS J1033+1809†	6070.0	− 8.55	0.24	− 8.04	0.24	0.31	0.25
SDSS J1038−0036†	7700.0	− 7.85	0.06	− 7.4	0.06	0.35	0.06
SDSS J1038+0432†	6510.0	− 7.50	0.16	− 6.99	0.16	0.31	0.16
SDSS J1040+2407†	5750.0	− 8.20	0.10	− 7.59	0.10	0.25	0.08
SDSS J1041+3432†	7500.0	− 8.20	0.19	− 7.29	0.19	0.12	0.08
SDSS J1043+3516†	6720.0	− 8.88	0.12	− 7.2	0.12	0.02	0.01
SDSS J1055+3725†	5600.0	− 8.24	0.14	− 7.83	0.14	0.39	0.18
SDSS J1058+3143†	6850.0	− 9.02	0.09	− 8.01	0.09	0.10	0.03

Table A1 – *continued*

Name	$T_{\rm eff}$ K	Ca/H(e) dex	$\sigma_{\rm Ca}$ dex	Fe/H(e) dex	$\sigma_{\rm Fe}$ dex	Ca/Fe	$\sigma_{\rm Ca/Fe}$
SDSS J1102+0214†	5730.0	− 9.75	0.10	− 8.74	0.10	0.10	0.03
SDSS J1103+4144†	5850.0	− 9.30	0.11	− 8.04	0.11	0.05	0.02
SDSS J1112+0700†	7560.0	− 8.53	0.15	− 7.37	0.15	0.07	0.03
SDSS J1134+1542†	6680.0	− 8.46	0.24	− 7.35	0.24	0.08	0.06
SDSS J1144+1218†	5434.0	− 9.33	0.11	− 8.37	0.11	0.11	0.04
SDSS J1144+3720†	7490.0	− 8.17	0.17	− 7.16	0.17	0.10	0.05
SDSS J1149+0519†	7310.0	− 8.16	0.12	− 7.6	0.12	0.28	0.11
SDSS J1150+4928†	7210.0	− 8.76	0.14	− 7.65	0.14	0.08	0.04
SDSS J1158+0454†	5270.0	− 8.69	0.22	− 7.58	0.22	0.08	0.05
SDSS J1158+1845†	7250.0	− 7.75	0.15	− 6.84	0.15	0.12	0.06
SDSS J1158+4712†	7650.0	− 8.06	0.18	− 6.85	0.18	0.06	0.04
SDSS J1158+5942†	6000.0	− 8.98	0.18	− 8.02	0.18	0.11	0.06
SDSS J1205+3536†	6070.0	− 8.74	0.16	− 7.63	0.16	0.08	0.04
SDSS J1211+2326†	6450.0	− 8.59	0.23	− 7.28	0.23	0.05	0.04
SDSS J1217+1157†	6440.0	− 8.93	0.14	− 7.92	0.14	0.10	0.05
SDSS J1218+0023†	6100.0	− 9.61	0.09	− 8.9	0.09	0.19	0.06
SDSS J1220+0929†	6640.0	− 8.38	0.14	− 7.37	0.14	0.10	0.05
SDSS J1224+2838†	5210.0	− 10.00	0.13	− 8.89	0.13	0.08	0.03
SDSS J1229+0743†	6160.0	− 8.20	0.13	− 7.09	0.13	0.08	0.03
SDSS J1230+3143†	6510.0	− 9.12	0.16	− 8.21	0.16	0.12	0.06
SDSS J1234+5208†	7630.0	− 7.40	0.09	− 6.39	0.09	0.10	0.03
SDSS J1238+2149†	5440.0	− 9.11	0.22	− 8.0	0.22	0.08	0.06
SDSS J1245+0822†	6360.0	− 8.10	0.19	− 7.59	0.19	0.31	0.19
SDSS J1254+3551†	6620.0	− 8.96	0.21	− 7.75	0.21	0.06	0.04
SDSS J1257−0310†	6280.0	− 8.52	0.23	− 7.31	0.23	0.06	0.05
SDSS J1259+3112†	5840.0	− 9.65	0.26	− 8.14	0.26	0.03	0.03
SDSS J1303+4055†	6200.0	− 9.02	0.12	− 8.11	0.12	0.12	0.05
SDSS J1308+0258†	6030.0	− 9.07	0.22	− 7.66	0.22	0.04	0.03
SDSS J1316+1918†	5350.0	− 9.90	0.23	− 8.99	0.23	0.12	0.09
SDSS J1319+3641†	7360.0	− 8.60	0.16	− 7.49	0.16	0.08	0.04
SDSS J1329+1301†	6810.0	− 8.55	0.14	− 7.44	0.14	0.08	0.04
SDSS J1330+3029†	6100.0	− 8.40	0.06	− 7.3	0.06	0.08	0.02
SDSS J1336+3547†	6600.0	− 8.50	0.07	− 7.39	0.07	0.08	0.02
SDSS J1339+2643†	6300.0	− 9.13	0.07	− 8.6	0.07	0.30	0.07
SDSS J1340+2702†	7855.0	− 6.98	0.22	− 6.27	0.22	0.19	0.14
SDSS J1345+1153†	6020.0	− 8.10	0.21	− 6.89	0.21	0.06	0.04
SDSS J1347+1415†	6740.0	− 8.50	0.11	− 7.29	0.11	0.06	0.02
SDSS J1350+1058†	5120.0	− 10.06	0.20	− 8.75	0.20	0.05	0.03
SDSS J1351+2645†	5980.0	− 8.04	0.17	− 7.53	0.17	0.31	0.17
SDSS J1356+0236†	8260.0	− 7.52	0.15	− 6.41	0.15	0.08	0.04
SDSS J1356+2416†	6030.0	− 9.20	0.13	− 8.54	0.13	0.22	0.09
SDSS J1401+3659†	6000.0	− 9.80	0.11	− 8.94	0.11	0.14	0.05
SDSS J1404+3620†	5900.0	− 9.20	0.08	− 8.5	0.08	0.20	0.05
SDSS J1405+1549†	7150.0	− 8.25	0.10	− 7.14	0.10	0.08	0.03
SDSS J1405+2542†	5880.0	− 9.50	0.20	− 8.39	0.20	0.08	0.05
SDSS J1411+3410†	5480.0	− 8.40	0.24	− 7.39	0.24	0.10	0.08
SDSS J1421+1843†	7300.0	− 7.35	0.18	− 6.19	0.18	0.07	0.04
SDSS J1428+4403†	6600.0	− 8.98	0.06	− 8.4	0.06	0.26	0.05
SDSS J1430−0151†	6150.0	− 7.55	0.16	− 6.99	0.16	0.28	0.14
SDSS J1445+0913†	6580.0	− 7.98	0.22	− 6.77	0.22	0.06	0.04
SDSS J1448+1047†	6550.0	− 8.85	0.09	− 7.8	0.09	0.09	0.03
SDSS J1502+3744†	5410.0	− 10.00	0.12	− 8.99	0.12	0.10	0.04
SDSS J1518+0506†	5020.0	− 9.65	0.13	− 8.74	0.13	0.12	0.05
SDSS J1524+4049†	5900.0	− 8.90	0.12	− 7.79	0.12	0.08	0.03
SDSS J1535+1247†	5773.0	− 8.61	0.05	− 7.57	0.05	0.09	0.02
SDSS J1542+4650†	6060.0	− 8.15	0.23	− 7.04	0.23	0.08	0.06
SDSS J1545+5236†	5840.0	− 9.19	0.13	− 8.18	0.13	0.10	0.04
SDSS J1546+3009†	6600.0	− 8.40	0.12	− 7.19	0.12	0.06	0.02
SDSS J1549+2633†	6290.0	− 9.66	0.18	− 8.25	0.18	0.04	0.02
SDSS J1554+1735†	6630.0	− 8.60	0.07	− 7.64	0.07	0.11	0.02
SDSS J1604+1830†	6400.0	− 9.48	0.12	− 8.57	0.12	0.12	0.05
SDSS J1616+3303†	6400.0	− 8.25	0.08	− 7.14	0.08	0.08	0.02
SDSS J1626+3303†	6260.0	− 8.87	0.25	− 7.61	0.25	0.05	0.05
SDSS J1627+4646†	6420.0	− 8.88	0.20	− 7.62	0.20	0.05	0.04

Table A1 – *continued*

Name	$T_{\rm eff}$ K	Ca/H(e) dex	$\sigma_{\rm Ca}$ dex	Fe/H(e) dex	$\sigma_{\rm Fe}$ dex	Ca/Fe	$\sigma_{\rm Ca/Fe}$
SDSS J1636+1619[†]	4410.0	− 9.50	0.21	− 8.79	0.21	0.19	0.13
SDSS J1641+1856[†]	5820.0	− 10.30	0.11	− 9.59	0.11	0.19	0.07
SDSS J1649+2238[†]	5332.0	− 8.62	0.18	− 7.21	0.18	0.04	0.02
SDSS J1706+2541[†]	6640.0	− 9.40	0.25	− 8.89	0.25	0.31	0.25
SDSS J2109−0039[†]	6040.0	− 8.78	0.25	− 7.67	0.25	0.08	0.06
SDSS J2123+0016[†]	5230.0	− 10.01	0.17	− 8.5	0.17	0.03	0.02
SDSS J2157+1206[†]	6100.0	− 9.00	0.10	− 8.09	0.10	0.12	0.04
SDSS J2225+2338[†]	7000.0	− 8.81	0.12	− 7.8	0.12	0.10	0.04
SDSS J2231+0906[†]	5900.0	− 9.85	0.09	− 8.84	0.09	0.10	0.03
SDSS J2235−0056[†]	6340.0	− 8.67	0.20	− 7.26	0.20	0.04	0.03
SDSS J2238−0113[†]	6800.0	− 8.89	0.25	− 7.78	0.25	0.08	0.06
SDSS J2238+0213[†]	7000.0	− 8.56	0.23	− 7.3	0.23	0.05	0.04
SDSS J2304+2415[†]	5060.0	− 9.54	0.13	− 8.93	0.13	0.25	0.10
SDSS J2319+3018[†]	7120.0	− 8.53	0.18	− 7.37	0.18	0.07	0.04
SDSS J2330+2805[†]	6670.0	− 8.84	0.20	− 7.63	0.20	0.06	0.04
SDSS J2340+0124[†]	6200.0	− 8.50	0.10	− 7.9	0.10	0.25	0.08
SDSS J2340+0817[†]	5550.0	− 9.00	0.14	− 7.69	0.14	0.05	0.02
SDSS J2352+3344[†]	7230.0	− 8.26	0.20	− 7.05	0.20	0.06	0.04
SDSS J2357+2348[†]	6030.0	− 9.07	0.25	− 7.76	0.25	0.05	0.04
NLTT 1675[ϕ]	9999.0	− 9.53	0.03	− 8.63	0.13	0.13	0.04
NLTT 6390[ϕ]	999.0	− 10.00	0.04	− 8.57	0.11	0.04	0.01
NLTT 19686[ξ]	999.0	− 8.70	0.04	− 8.93	0.14	1.70	0.57

Note. [α]Jura et al. (2012) [β]Farihi et al. (2013) [γ]Dufour et al. (2012) [ϵ]Xu et al. (2013) [ζ]Zuckerman et al. (2011) [η]Klein et al. (2011) [θ]Raddi et al. (2015) [ι]Farihi et al. (2016) [κ]Wilson et al. (2015) [λ]Gänsicke et al. (2012) [†]Hollands et al. (2017) [ϕ]Kawka & Vennes (2012) [ξ]Kawka & Vennes (2016) [*]Swan et al. (2019) [z]Jura et al. (2012); Zuckerman et al. (2010)

This paper has been typeset from a TEX/LATEX file prepared by the author.